

Passive Control of Cavity Flows

S. Yamouni, C. Mettot
D. Sipp, L. Jacquin
(Onera)

E-mail: denis.sipp@onera.fr

This paper deals with cavity flow physics and its passive control by means of a spanwise cylinder. Two configurations are considered. First, a laminar study of a flow over an unconfined square cavity at a low Reynolds number (7500) is presented. Global stability results are shown, allowing the identification of the driving mechanisms of the cavity flow: the aeroacoustic feedback mechanism ([18]) and the acoustic resonance mechanism [4]. When both mechanisms interact, the growth rate of the global modes is seen to display a local maximum. At low Mach numbers, we suggest that it is still the feedback aeroacoustic mechanism that selects the frequency mode, the acoustic resonance mechanism only enhancing the response. Second, we study the dynamics of a turbulent deep cavity flow in a transonic regime. Global modes and sensitivity results are shown and compared to experimental data, with and without control cylinder. Concerning the baseline (without control), RANS and URANS simulations, based on the $k-\omega$ model of Wilcox, display very good agreement with experiments. Also, the sensitivity map obtained numerically is extremely close to the experimental control map obtained by moving a small control cylinder in the upstream boundary layer and the shear-layer. Different interpretation elements are discussed.

Cavity flows as a source of unsteady loads and noise

Historical note

The flow that develops over an open cavity is a generic example of self-sustained fluidic oscillations. Other flows of this type are shock oscillations on the suction side of a wing profile at a high (subsonic) Mach number and high angles of attack, impinging jets, combustion instability phenomena, or bluff bodies. These self-sustained oscillating flows result from complex interactions between fundamental mechanisms comprising hydrodynamic instabilities, vortex dynamics, acoustic wave propagation and turbulence. In the compressible regime, the impingement of vortices induced by Kelvin-Helmholtz instabilities, which develop in the shear-layer over the cavity, generates acoustic pressure waves travelling upstream. These pressure waves excite the Kelvin-Helmholtz instabilities, which closes the feedback loop. As a result, specific frequencies are selected. This interaction can be the source of unsteady loads and noise, which can be detrimental to the obstacle surroundings. Indeed, even if the acoustic energy only represents a weak part of the total mechanical energy of the system ($E_{ac} \approx 10^{-5} E_{total}$), high acoustic levels can be reached. Cavity flows have been studied since the 1950s, motivated by aeroacoustics, aero-elasticity and aero-optics applications. In military applications [6], [8], weapon bays are subjected to oscillations that can enter in resonance with the modes of the aircraft structure. Image distortion due to cavity flow effects is a great concern for in-born observations. During the landing and take-off of transport aircraft,

landing gears are important sources of noise [7]. Cavity flow phenomena also concern ground transportation. Car sun-roofs and windows, and the shallow cavities receiving the pantograph in trains are classical examples.

Driving mechanisms

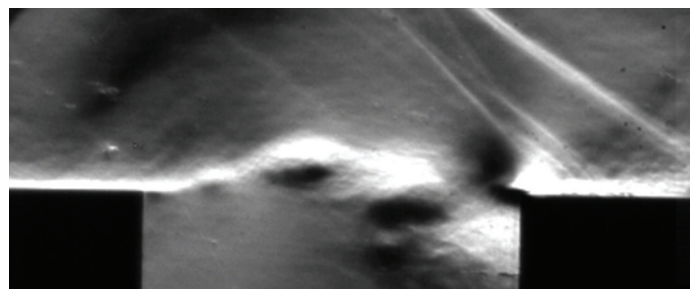


Figure 1 - Schlieren picture of an uncontrolled cavity flow at $M=0.8$

In a cavity flow, it is generally acknowledged that two physical mechanisms are at play. First, the feedback aeroacoustic mechanism, described by [18], induces self-sustained oscillations. Small disturbances are amplified along the shear layer by the Kelvin-Helmholtz instability and convected downstream. The impact of these structures upon the cavity trailing edge leads to the formation of acoustic waves traveling upstream up to the sensitive region located at the leading edge. This process is visible in figure 1, where the large vortical structures of the shear layer and the pressure waves are clearly

visible thanks to a Schlieren system. Second, [4] modeled empirically the resonant response of deep cavities, which is linked to the presence of acoustic standing-waves inside the cavity. Henceforth, this phenomenon is referred to as the acoustic resonance mechanism. This phenomenon occurs when the acoustic wavelength is of the same order as the length (or depth) of the cavity. The feedback aeroacoustic mechanism can be enhanced by acoustic standing-wave resonances [17]. However, [25] stated that a theory combining both mechanisms is still lacking.

Recent advances improving the understanding of cavity flow physics are described in the section “The physics of cavity flows: new results” [26], [27]. We will show that a global stability analysis is a relevant theory to, first, capture the two aforementioned mechanisms, the feedback aeroacoustic and the acoustic resonance mechanisms, and second, to show that a similar mechanism is at play in the incompressible and the compressible regimes.

Control of cavity noise

Many control techniques have been tested in order to reduce the cavity acoustic tones with variable results. Both active and passive control systems have been used (see article review of [2]). Passive control devices are the easiest to implement and a wide variety of systems were tested, in particular: spoilers, mass injection and modification of the cavity leading and/or trailing edge. These concepts sometimes proved to be very effective in reducing energetic tones but, in general, they did not succeed in suppressing multiple acoustic modes simultaneously. The effect of a spanwise cylinder in compressible crossflow parallel to the leading edge of the cavity is another passive device that proved to be very efficient, as shown first by [13]. This control system has been subsequently described by [22], [23], [9] and [15]. Some active control methods have been also tested, where small amplitude disturbances are introduced by means of unsteady flow injections or flapping actuator devices. Control by open-loop forcing or feedback control strategies have been also tested [19], [20].

In [28], an experiment was performed where the evolution of the pressure spectrum energy was measured as a function of the cylinder position within the upstream boundary layer and the shear layer of the cavity. This experiment will be described in the section “The passive control of cavity flows”. From this experiment, a sensitivity map that favorably compares with the theory was deduced, showing that the regions where cavity tones are controlled are the regions where the global modes are stabilized.

The physics of cavity flows: new results

As mentioned above, cavity flow physics stems from a global mechanism that couples hydrodynamics (the shear layer) and acoustics (pressure waves). Note that a local approach for the hydrodynamic part is not recommended due to the global nature of this physics. A global approach based on a hydrodynamic global stability analysis also successfully described the dynamics of other flows, such as shock-induced transonic-buffet [3], shock wave/laminar boundary layer interaction [16], flow around a swept parabolic body [11] or axisymmetric wake flows [14].

In this section, we will present results using the global stability analysis for two cavity cases [27], [28].

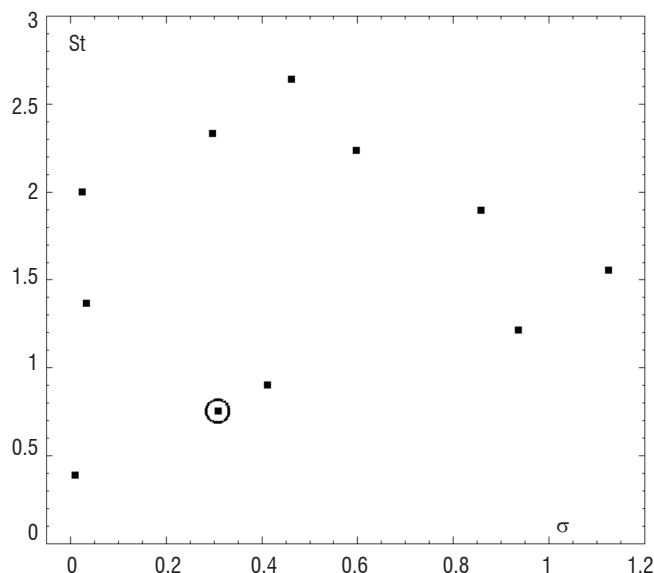


Figure 2 - Spectrum of the unstable global modes obtained at $M=0.8$ [27]

Global modes: principle

The equations governing the flow dynamics can be written in the form

$$\partial_t W = R(W) \quad (1)$$

where W represents the aerodynamic field and $R(W)$ represents the residual. W denotes either the divergence-free velocity field in the case of the incompressible Navier-Stokes equations ($W = (\mathbf{U}, \mathbf{p})^T$), or a set of variables containing the density, the velocity field and the energy in the compressible case ($W = (\rho, \mathbf{U}, T)^T$).

The base flow W_0 , an equilibrium point of eq. (1), is defined by:

$$R(W_0) = 0 \quad (2)$$

The dynamics of the small perturbations w superimposed on this field are governed by $\partial_t w = A(w)$, where A is the Jacobian operator

linked to the residuals R by the relation $A = \left. \frac{\partial R}{\partial W} \right|_{W_0}$.

The perturbation is then sought in the form of normal modes $w(x, y, t) = \hat{w}(x, y)e^{(\sigma+i\omega)t}$, where σ and ω represent the temporal growth rate and the frequency of the global mode \hat{w} , respectively. When $\sigma > 0$ (resp. < 0), the base flow is unstable (resp. stable). Substituting w leads to a generalized eigenvalue problem for $\lambda = \sigma + i\omega$ and \hat{w} :

$$A\hat{w} = \lambda\hat{w} \quad (3)$$

In figure 2, an example of global spectrum obtained at $M=0.8$ is displayed in the (σ, St) plane. There are eleven unstable modes whose convergence has been checked by varying the mesh refinement [27].

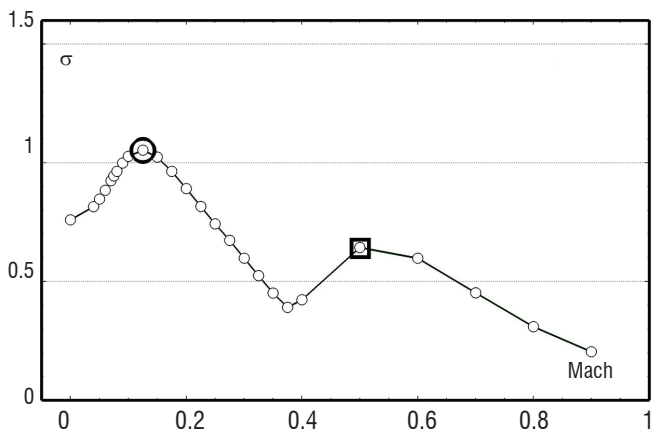


Figure 3 - Temporal growth rate evolution of the unstable global mode $n=2$ as a function of the Mach number [27].

Mach effects on the global modes

In this paragraph, new insights on the cavity dynamics are presented. They concern the dependency of the unstable global modes with the Mach number and the link between the incompressible and the compressible regimes. Results are extracted from [27] dealing with a laminar flow passing above an unconfined square cavity. The Reynolds number based on the cavity length is set at $Re_L = 7500$, sufficient to be unstable [21], while the Mach number has been varied from the incompressible regime ($M=0$) to high subsonic compressible regime ($M=0.9$).

Interaction between feedback aeroacoustic mechanism and acoustic resonance mechanism

The interaction phenomenon between the feedback aeroacoustic and acoustic resonance mechanisms has already been observed in experiments and simulations by monitoring acoustic pressure levels. For example, in the case of a deep cavity of length-to-depth ratio equal

to 0.66, [1] analyzed the pressure spectrum by varying the Mach number between low Mach numbers up to $M=0.5$. Block observed several peaks evolving as a function of the Mach number and noticed that the amplitude of these peaks is the greatest when the aeroacoustic feedback curves ($n=1, 2$) (see Eq. (4)) match with the first acoustic resonance curve of [4]. The aeroacoustic feedback mechanism has been formulated by [1] as,

$$St = \frac{n - \gamma}{\frac{1}{\kappa} + M} \quad (4)$$

where n is the mode number, κ is the ratio between the convection speed of the vortices and the free-stream velocity, M is the Mach number and γ is a delay time ($\gamma < 1$).

[27] tracked the eigenvalues by varying the Mach number. In figure 3, one trajectory ($n=2$) has been represented in the ($M; \sigma$) plane. Note that the Strouhal number varies along such a curve. The authors observed that, for intermediate Mach numbers, the trajectory displays two local maxima in the growth rate, corresponding to the match between both mechanisms in accordance with experimental evidence.

Link between the incompressible and the compressible regimes

Initially, the feedback aeroacoustic model proposed by [18] was made to match the mode evolution as a function of the Mach number (see Eq. (4)), and was restricted to the compressible regime. In the incompressible regime, where the pressure feedback is instantaneous, its applicability remains controversial. However, in [27], the authors argue that the feedback aeroacoustic mechanism is also valid in the incompressible regime. They first showed that the frequency and the shape of the unstable global modes in the incompressible case are very similar to the ones observed at very low Mach numbers. Second, thanks to spatio-temporal ($x-t$) diagrams such as those displayed in figure 4, they showed that a common mechanism is at play throughout the entire range of subsonic Mach numbers, from $M=0$ to $M=0.8$. This figure displays the pressure of the global modes

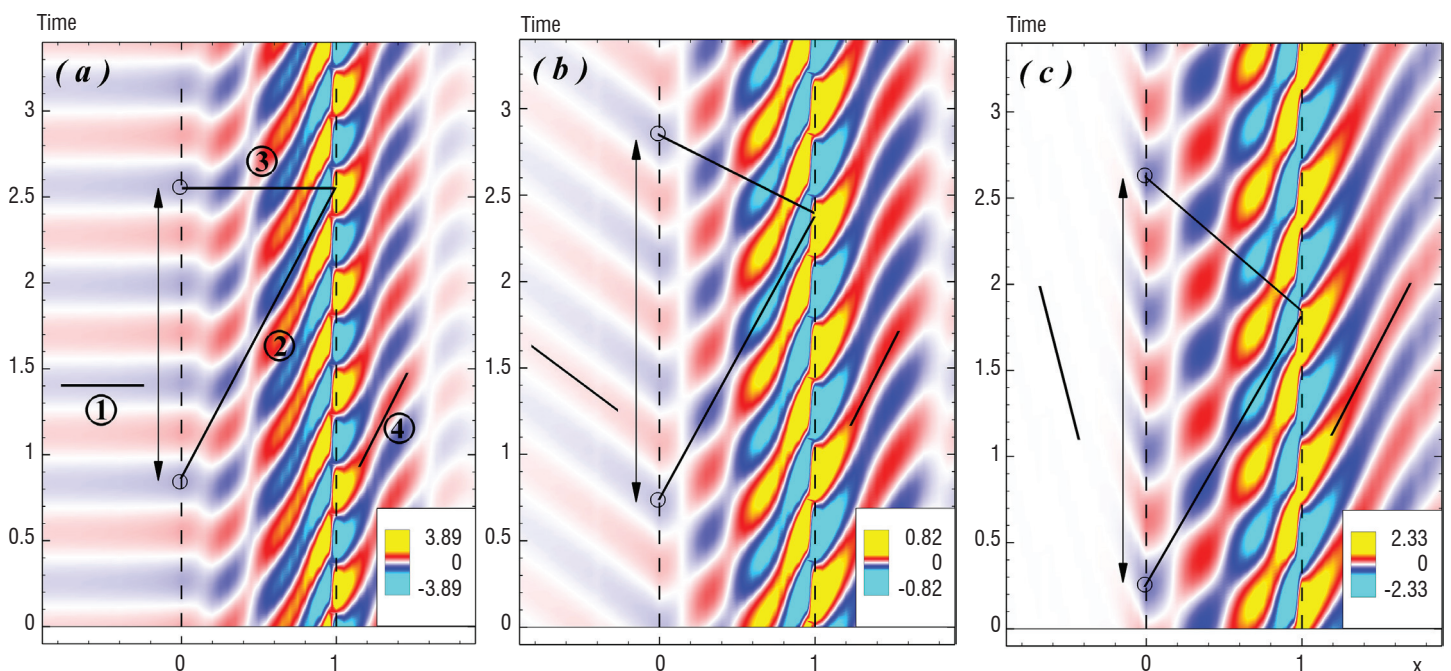


Figure 4 - Spatio-temporal diagrams of the modes belonging to branch $n=3$ showing the pressure extracted on a segment at $y=0$. Three Mach numbers are displayed: (a) $M=0$, (b) $M=0.4$, (c) $M=0.8$.

lying on branch $n=3$ (see Eq. (4)), extracted at the cavity mouth ($y=0$). The leading ($x=0$) and downstream ($x=1$) edges of the cavity are identified by the dashed lines. The slopes of the elongated blue line patterns denote the celerity of the pressure waves. For x in $[0;1]$ and $y=0$, the pressure of the global modes is characterized by patterns that are pressure fluctuations associated with the vortical structures of the mixing layer. For $x \leq 0$, the patterns are uniquely due to acoustic pressure waves. For instance, considering the slope of the lines labeled ②, the convective velocity of the vortices inside the shear layer is nearly constant and independent of the Mach number value. Differences are only observed in the return speed of the feedback pressure wave (lines labeled ③), which is infinite for $M=0$ and finite for $M > 0$. This shows that the basic physics is the same for incompressible and compressible flows.

Turbulent regimes

The previous section dealt with laminar flows. Accounting for turbulence is necessary when dealing with an experiment such as the one that we are going to describe. Specific CFD tools are required. For the latter, we use a RANS code (*e/sA*, the Onera CFD suite) for the base flow and global mode calculation. The base flow is still a steady solution of the Navier-Stokes equations, obtained from the convergence of RANS simulations. The URANS version of the code is also used to check good agreement with the experiment.

In this section, stability calculations, unsteady simulations, both based on RANS equations using the $k-\omega$ model of Wilcox and comparison with experiment are shown. Sensitivity maps are established from both calculation and experiment. The results are extracted from [28].

Flow configuration

The cavity is that studied by [5], [10] and [28]. It is a deep cavity with a length-to-depth ratio of $L/D=0.42$. The Mach number is equal to 0.76 and the Reynolds number, based on the cavity length, is equal to $Re_L = 815000$. The boundary layer thickness at the cavity leading edge is $\delta_0 \approx 10$ mm. Numerical simulations were also performed, using the same geometry, with a Mach number of 0.8, a Reynolds number equal to $Re_L = 860000$ and a turbulent upstream boundary

layer thickness set at $\delta_0 \approx 2.3$ mm. In both cases, the reference pressure signal is P_{Ref} located at the downstream cavity edge ($x=50; z=-0.5$ mm).

Interpretation of the cavity dynamics with global modes

In figure 5(a), the unstable global modes obtained from the stability calculations (see the section "Global modes: Principle") are displayed. Within the framework of the RANS equations with the Wilcox $k-\omega$ model, a set of conservative variables is used ($W = (\rho, \rho U, \rho E, \rho k, \rho \omega)^T$), where E represents the total energy, k , the turbulent kinetic energy, and ω represents the specific dissipation rate. Two types of global modes are obtained: the first type called the "Kelvin-Helmholtz branch" (red circled symbols) displays modes with shear layer instabilities; the second type comprises the acoustic modes, which exhibit lower but non-zero temporal growth rates σ , since they result from the interaction with hydrodynamic structures. These modes display an intense resonant structure inside the cavity and in the tunnel [26] and [28]. One notes the similarity between this global spectrum and the one displayed in figure 2, in the case of a laminar flow at the same Mach number $M=0.8$, despite the huge difference in the Reynolds numbers. The frequency of the modes lying on the "Kelvin-Helmholtz branch" is similar, while the general growth rate levels are weaker in the turbulent case, due to eddy viscosity effect. In figure 6, the spatial structure of two unstable global modes is shown through the density: the first is the lowest Strouhal mode ($\sigma=0.13; St=0.40$) (a) and the second is the most unstable mode ($\sigma=0.62; St=1.5$) (b). Both belong to the "Kelvin-Helmholtz branch". The mode structure is similar to the one presented in [27], displaying vortical structures in the shear layer and acoustic pressure waves with a resonance pattern inside the cavity.

Returning to figure 5(b), the spectrum of the downstream pressure sensor, P_{Ref} obtained with unsteady RANS simulations, is compared with the experimental one. Good agreement is found for the peak frequencies up to the fifth harmonic, whereas the sound pressure level is overestimated in the numerical simulation, with a difference of nearly 10 dB regarding the fundamental peak ($St \approx 0.4$). In the same figure, the dashed horizontal lines represent the frequencies of the unstable global modes lying on the "Kelvin-Helmholtz branch" displayed

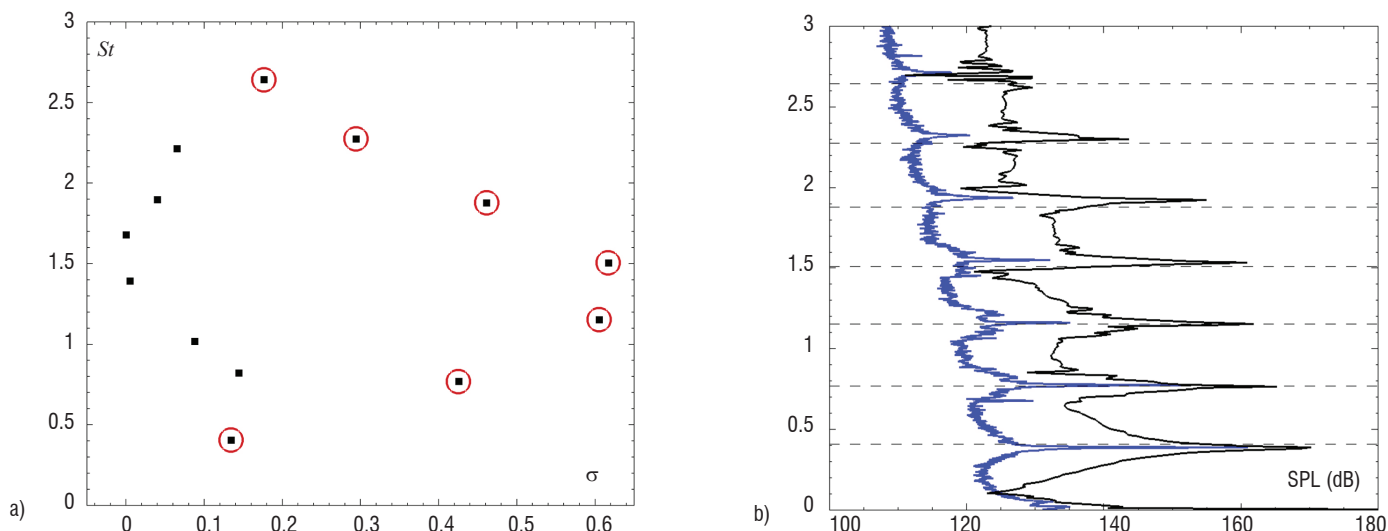


Figure 5 - Comparison between (a) the spectrum of the unstable global modes and (b) the spectra obtained from the URANS simulation (black solid lines) and experiments (blue solid lines). The red circled symbols in (a) are the modes lying on the "Kelvin-Helmholtz branch" and the dashed lines in (b) correspond to the frequencies of these modes.

in figure 5(a). Again, the agreement is very good, which proves that a global stability analysis is able to predict the frequency of the shear layer modes.

In conclusion, the main physics of the cavity, as described by the global mode approach, is very poorly dependent on turbulence. The latter only alters the growth rate of the global modes.

The passive control of cavity flows

In this last section, experimental and numerical results based on the same configuration as above are considered, with the presence of a passive control cylinder.

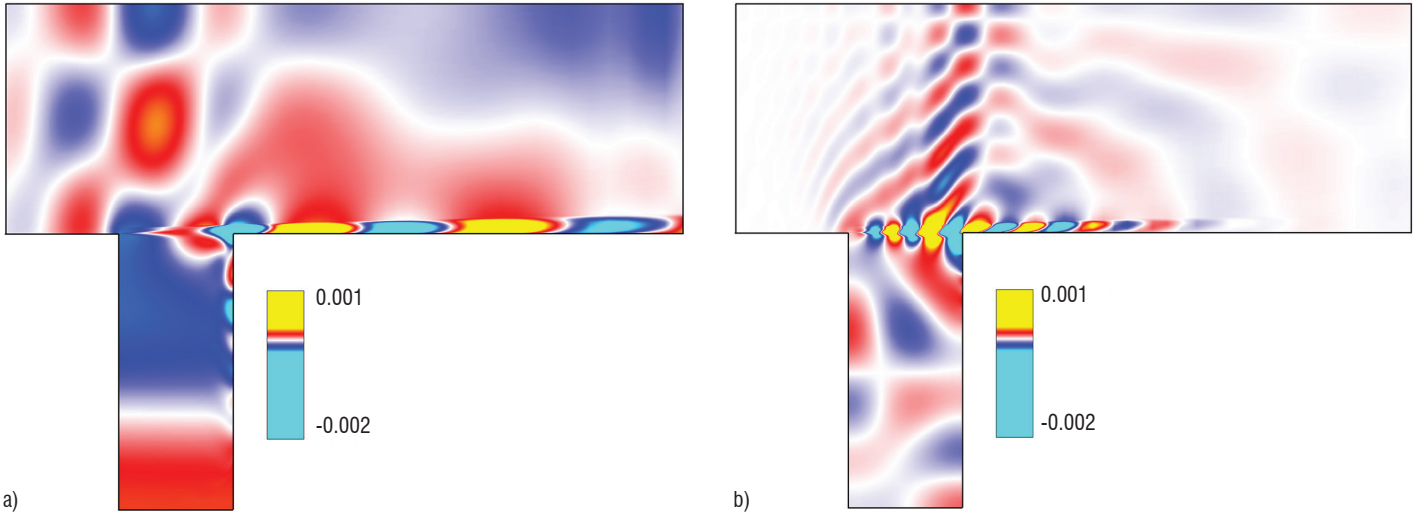


Figure 6 - Spatial distribution of density for the two unstable global modes (0.13; 0.40)(a) and (0.62;1.5)(b).

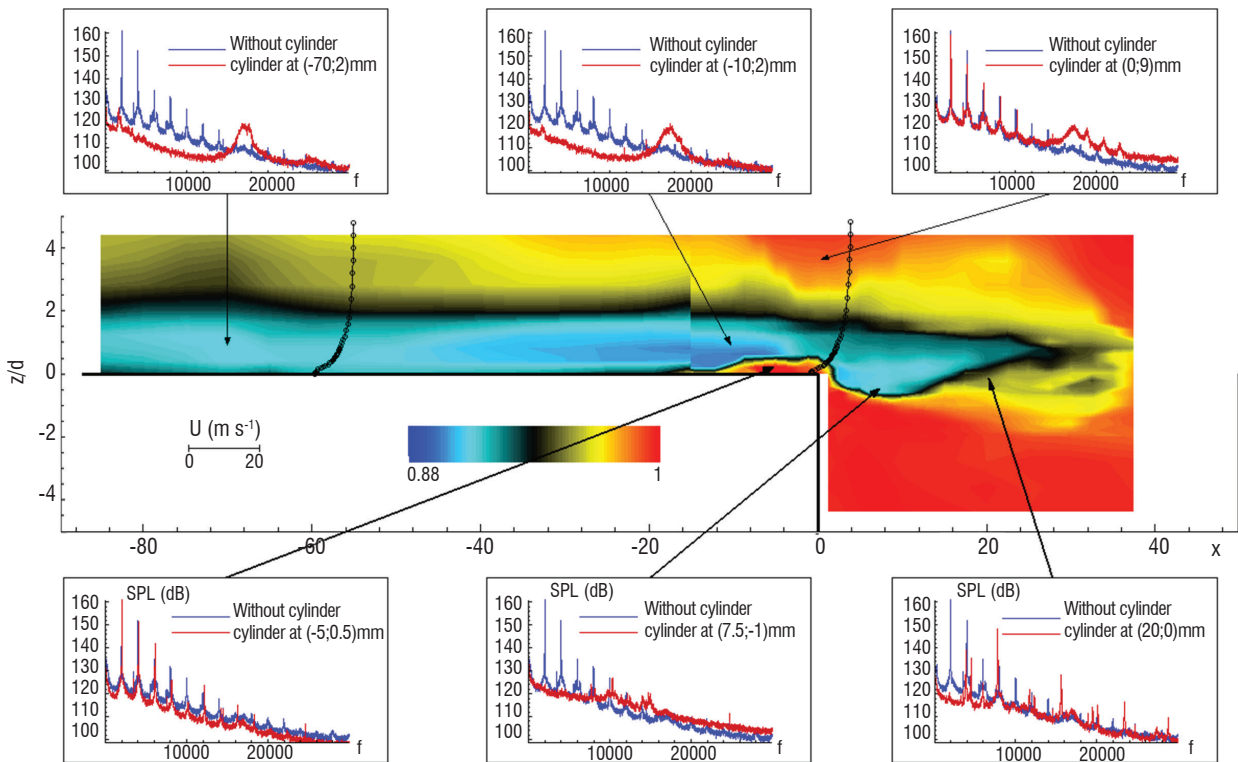


Figure 7 - Control map obtained by integrating the pressure spectrum of the reference sensor P_{Ref} located at the downstream cavity edge (50; -5) mm. All around the map, pressure spectra are displayed, comparing the reference case with the cylinder to controlled cases. The arrows indicate the cylinder position in the map for each spectrum.

Experimental control map

To make the cavity control map, the cylinder ($d=2.5$ mm) is moved within both the upstream boundary layer and the shear layer. The acoustic energy of the reference pressure sensor P_{Ref} located at the downstream cavity edge ((50; -5) mm), is calculated for each position of the cylinder. It is then compared with the acoustic energy of the cavity without cylinder. In figure 7, the control map of the cylinder, i.e., the ratio of the acoustic energy between the controlled and the uncontrolled situation, is displayed. In the blue regions, the control cylinder is effective in reducing the acoustic energy, while it is not in the red regions. First, we observe that, for $x < -10$ mm, the control is effective in the entire upstream boundary layer for $z_d/d < 2$. Looking at the position $x=-5$ mm, we retrieve the results from [10]: the control fails if $z_d/d \leq 0.4$ and $z_d/d \geq 2$. Second, the control is also effective in the upstream part of the shear layer for z_d/d in $[-0.7; 1.2]$ and x up to 25 mm.

Sound Pressure Level spectra (in dB), comparing the reference case to the controlled cases for different cylinder positions, are also displayed in figure 7. Control may lead to a reduction of the dominant cavity tones from 160 dB to 120 dB (see control location (-10;2) mm). The control efficiency seems to be related to the strength of the Von-Karman vortex shedding, which may be monitored at P_{Ref} . The cylinder Von-Karman frequency ($St=fd/U_\infty \approx 0.2$) is visible for the control locations $(x,z)=(-70;2)$ mm and $(-10;2)$ mm, for which the control is effective. Also, it is seen that the control is ineffective when the cylinder Von-Karman frequency is not seen (see location $(x,z)=(-5;0.5)$ mm), or when the control cylinder wake does not directly interact with the mixing-layer (see location $(x,z) = (0;9)$ mm). Hence, the control is effective when the turbulent stresses associated to the Von-Karman vortex street efficiently diffuse the mixing layer and thus change the mean-flow. However, this appears not to be true when the control cylinder is located at $(x,z) = (7.5;-1)$ mm in the shear-layer. There it is seen that the flow may be efficiently manipulated while the cylinder Von-Karman frequency is only barely seen at P_{Ref} . These observations suggest that the addition of the small cylinder controls the flow by modifying the stability of the mean velocity field. To confirm this, in the following section we have performed a sensitivity study of the unstable eigenvalues to a steady forcing.

Comparison with numerical sensitivity

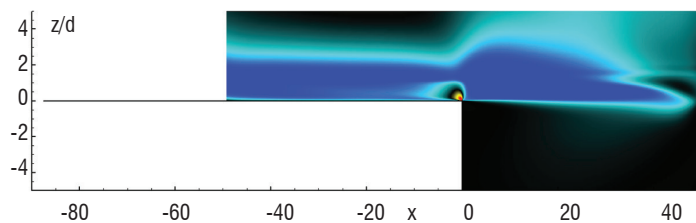


Figure 8 - Sensitivity map of the lowest Strouhal mode (0.13; 0.40) (see figure 6(a)), displaying the growth rate sensitivity ($\delta\sigma$) to a steady forcing δf , imitating the effect of a small cylinder on the flow.

References

- [1] P. J.W. BLOCK – *Noise Response of Cavities of Varying Dimensions at Subsonic Speeds*. Technical Report D-8351, N.A.S.A. Tech. Note, 1976
- [2] L.N. CATTAFESTA III, Q. SONG, D.R. WILLIAMS, C.W. ROWLEY, F.S. ALVI - *Active Control of Flow-Induced Cavity Oscillations*. Progress in Aerospace Sciences, 44(7):479–502, 2008
- [3] JD CROUCH, A. GARBARUK, and D. MAGIDOV - *Predicting the Onset of Flow Unsteadiness Based on Global Instability*. AIAA paper 97-2004, 1997

In the case of the control of a cylinder wake by means of a small cylinder, [12] introduced a formalism able to predict the stabilizing regions identified by [24]. The idea is to consider the eigenvalue λ as a function of the base flow W_0 , which is itself a function of the steady forcing f , simulating the effect of a small cylinder. We wonder to what extent the application of a small amplitude steady force (δF) on the base flow (W_0) could modify the eigenvalue spectrum (λ). The sensitivity can then be expressed using a gradient formulation:

$$\delta\lambda = \langle \nabla_f \lambda, \delta f \rangle \quad (5)$$

where δf models the presence of a solid cylinder at the position (x_0, y_0) . Substituting $\delta f(x,y)$ in Eq. (5), the variation of the eigenvalue ($\delta\lambda(x_0, y_0)$) for a position of the control cylinder (x_0, y_0) is given by:

$$\delta f(x,y) = -U_0(x_0, y_0) \delta(x - x_0, y - y_0) \quad (6)$$

In figure 8, the sensitivity map of the lowest Strouhal mode ((0.13; 0.40) in figure 5(a)), showing where the control cylinder should be placed to stabilize the flow (real part of $\delta\lambda$), is displayed. It quantifies the modification induced by the steady forcing δf on this unstable global mode. The stabilization region, depicted in blue, contains the upstream boundary layer up to $x=-50$ mm (limit of the numerical domain), and one part of the shear layer. This control region is very similar to the experimental control region displayed in figure 7.

Conclusion

In this article, we first present results concerning a laminar case: the flow over an unconfined square cavity flow at a Reynolds number of 7500. Global stability results for Mach numbers ranging from $M=0$ to $M=0.9$. By analyzing the evolution of the growth rate (σ) and the frequency (ω) of the unstable global modes obtained, two main observations have been made. First, the unstable modes display a local growth rate maximum, where both driving mechanisms (the feedback aeroacoustic and the acoustic resonance mechanisms) intersect. Second, the applicability of the feedback aeroacoustic mechanism at very low Mach numbers, including the incompressible regime ($M=0$), has been exemplified at different Mach numbers thanks to spatio-temporal diagrams.

Then, results from numerical simulations, including global modes, unsteady simulations and sensitivity analysis, were compared to experimental data, with and without the passive control cylinder. It appears that the linear global stability analysis of RANS equations ($k-\omega$ model of Wilcox), is able to capture the unsteady non-linear cavity flow dynamics. Finally, the sensitivity analysis succeeded in predicting the stabilization region, where the flow is controlled by means of a small control cylinder ■

- [4] L.F. EAST - *Aerodynamically Induced Resonance in Rectangular Cavities*. J. Sound Vib., 3:277–287, 1966.
- [5] N. FORESTIER, L. JACQUIN, and P. GEFFROY - *The Mixing Layer over a Deep Cavity at High-Subsonic Speed*. Journal of Fluid Mechanics, 475:101–145, 2003
- [6] J.S. GIBSON - *Non-Engine Aerodynamic Noise Investigation of a Large Aircraft*. volume 2378. National Aeronautics and Space Administration, 1974
- [7] H.H. HELLER and W.M. DOBRZYNSKI - *Sound Radiation from Aircraft Wheel-Well/Landing-Gear Configurations*. J. Aircr, 14(8):768–774, 1977
- [8] H.H. HUBBARD - *Aeroacoustics of Flight Vehicles: Theory and Practice*. Volume 1. noise sources. Technical report, DTIC Document, 1991
- [9] H. ILLY - *Contrôle de l'écoulement au-dessus d'une cavité en régime transsonique*. PhD thesis, Université de Lyon, 2005.
- [10] H. ILLY, L. JACQUIN, and P. GEFFROY - *Observations on the Passive Control of Flow Oscillations over a Cavity in a Transonic Regime by Means of a Spanwise Cylinder*. AIAA paper, 5th AIAA Theoretical Fluid Mechanics Conference, 23-26 June 2008, Seattle, Washington, AIAA 2008-3774, 2008.
- [11] C.J. MACK, P.J. SCHMID, and J.L. SESTERHENN - *Global Stability of Swept Flow around a Parabolic Body: Connecting Attachment-Line and Crossflow Modes*. Journal of Fluid Mechanics, 611(1):205–214, 2008
- [12] O. MARQUET, D. SIPP, and L. JACQUIN - *Sensitivity Analysis and Passive Control of Cylinder Flow*. Journal of Fluid Mechanics, 615:221–252, 2008
- [13] S. MCGRATH and L. SHAW - *Active Control of Shallow Cavity Acoustic Resonance*. AIAA paper, 1996-1949, 1996
- [14] P. MELIGA, D. SIPP, and J.M. CHOMAZ - *Effect of Compressibility on the Global Stability of Axisymmetric Wake Flows*. J. Fluid Mech., 660:499–526, 2010
- [15] P. PANICKAR and G. RAMAN - *Understanding the Mechanism of Cavity Resonance Suppression using a Cylindrical Rod in Crossflow*. AIAA paper 2008-54, 2008
- [16] J.C. ROBINET - *Bifurcations in Shock-Wave/Laminar-Boundary-Layer Interaction: Global Instability Approach*. Journal of Fluid Mechanics, 579(1):85–112, 2007
- [17] D. ROCKWELL and E. NAUDASCHER - *Review - Self-Sustaining Oscillations of Flow Past Cavities*. Journal of Fluids Engineering, 100:152, 1978
- [18] J.E. ROSSITER - *Wind-Tunnel Experiments on the Flow over Rectangular Cavities at Subsonic and Transonic Speeds*. Technical report, Aero. Res. Council. R. & M., 1964
- [19] C.W. ROWLEY and D.R. WILLIAMS - *Dynamics and Control of High-Reynolds-Number Flow over Open Cavities*. Annu. Rev. Fluid Mech., 38:251–276, 2006
- [20] M. SAMIMI, M. DEBIASI, E. CARABALLO, A. SERRANI, X. YUAN, J. LITTLE, and JH MYATT - *Feedback Control of Subsonic Cavity Flows using Reduced-order Models*. Journal of Fluid Mechanics, 579:315, 2007.
- [21] D. SIPP AND A. LEBEDEV - *Global Stability of Base and Mean Flows: a General Approach and its Applications to Cylinder and Open Cavity Flows*. Journal of Fluid Mechanics, 593:333–358, 2007
- [22] M.J. STANEK, G. RAMAN, V. KIBENS, J.A. ROSS, J. ODEDRA, AND J.W. PETO - *Control of Cavity Resonance Through very High Frequency Forcing*. AIAA 2000-1905, 2000
- [23] M.J. STANEK, J.A. ROSS, J. ODEDRA, and J. PETO - *High Frequency Acoustic Suppression - the Mystery of the Rod-in-Crossflow Revealed*. In 41st AIAA Aerospace Sciences Meeting & Exhibit, Reno, NV, AIAA 2003-0007, 2003
- [24] PJ STRYKOWSKI and KR SREENIVASAN - *On the Formation and Suppression of Vortex 'Shedding' at Low Reynolds Numbers*. Journal of Fluid Mechanics, 218:71–107, 1990
- [25] C.K.W. TAM and P.J.W. BLOCK - *Tones Induced by Flow over Cavities*. J. Fluid Mech., 89:373–399, 1978
- [26] S. YAMOUNI - *Contrôle en boucle ouverte des instationnarités de cavité en régime transsonique*. PhD thesis, Ecole Polytechnique, Paris, 2013
- [27] S. YAMOUNI, D. SIPP, AND L. JACQUIN - *Interaction between Feedback Aeroacoustic and Acoustic Resonance Mechanisms in a Cavity Flow: a Global Stability Analysis*. Journal of Fluid Mechanics, 717:134–165, 2013
- [28] S. YAMOUNI, C. METTOT, D. SIPP, and L. JACQUIN - *Passive Control of a Transonic Deep Cavity Flow by Means of a Spanwise Cylinder*. In preparation for publication in Journal of Fluid Mechanics, 2013

Acronyms

RANS (Reynolds-Averaged Navier-Stokes)
uRANS (unsteady Reynolds-Averaged Navier-Stokes)
CFD (Computational Fluid Dynamics)

AUTHORS



Sami Yamouni graduated from “Supmecca Paris” in 2009. He joined Onera in the Fundamental/Experimental Aerodynamics Dept for his research internship regarding the control of cavity flow. He obtained his PhD in Fluid Mechanics from the Ecole Polytechnique in 2013. His research interests include Aeroacoustics, Hydrodynamic Stability, Compressible Flows, Aerodynamics and Experimental and Numerical activities.



Clément Mettot graduated from the Ecole Polytechnique and is currently doing his PhD in the Fundamental and Experimental Aerodynamics Department. His work concerns the passive control of turbulent flows, with the development of a numerical method to compute sensitivity gradients for turbulent flows.



Denis Sipp has been a researcher at Onera since 2002. He is the head of the Fluid Mechanics unit in the Fundamental and Experimental Aerodynamics Department. He obtained a PhD degree from the Ecole Polytechnique in 1999 on the stability of vortex pairs. He obtained his Habilitation Degree in 2009 at the Pierre et Marie Curie University in Paris. He has been a Professor (PCC) in the Mechanics Department of the Ecole Polytechnique since 2003.



Laurent Jacquin Research Director, Director of the Fundamental/Experimental Aerodynamics Dept of Onera. Associate Professor in Mechanical Engineering (from 1996 to 2007) and Professor in Fluid Mechanics at the Ecole Polytechnique. Background: Master's Degree in Mechanical Engineering from the University of Marseille. PhD from the University of Marseille in 1983. Research Habilitation Thesis (thèse d'état) from the University of Lyon in 1987. He joined Onera in 1987. His research topics include: Turbulence, Hydrodynamic Stability, Vortex Dynamics, Compressible Flows, Aerodynamics and Experimental Methods.